Macromolecular Research

Article

DOI 10.1007/s13233-020-8073-5

www.springer.com/13233 pISSN 1598-5032 eISSN 2092-7673

Ultrahigh Energy Storage Capacitance and High Breakdown Strength in Biaxially Oriented Poly(vinylidene fluoride) Using a High-Electric-Induced Technique

Hongwei Lu[1]
Jianxin Du[1]
Cuiping Yu[1]
Xingping Wang[4]
Yanlin Gao[4]
Weizhong Xu[3]
Aiping Liu[3]
Xiaoxiao Lu[1]
Yingxin Chen*[,1,2]

[1] College of Materials & Environmental Engineering, Hangzhou Dianzi University, Hangzhou 310018, P. R. China
[2] Key Laboratory of Optoelectronic Chemical Materials and Devices, Ministry of Education, School of Chemical and Environmental Engineering, Jianghan University, Wuhan 430056, P. R. China
[3] Nanometer Measurement Laboratory, Center for Optoelectronics Materials and Devices, Zhejiang Sci-Tech University, Hangzhou 310018, P. R. China
[4] Engineering Technology Research Center of Fluoro-material, Quzhou 324004, P. R. China

Received july 14, 2019 / Revised October 19, 2019 / Accepted November 5, 2019

Abstract: The development of high dielectric materials with high energy densities is a crucial research domain in the modern microelectronics and power systems. The objective of this work was to develop the highly ordered crystal orientations and large ferroelectric crystalline β/γ-phases in the biaxially oriented poly(vinylidene fluoride) (BOPVDF). Importantly, a high discharged energy density and high dielectric constant was achieved by using a high-electric-induced technique. A suitable poling electric field was applied to the BOPVDF films in order to enhance the breakdown strength. Remarkably, the BOPVDF film poled at the electric field of 113 MV m^{-1} achieved an unprecedented discharged energy density of 25.4 J cm^{-3} at an ultra-high electric field of 550 MV m^{-1}, which is by far the highest value ever achieved in flexible polymer-based capacitor films. Comparatively, the unpoled BOPVDF and commercial biaxially oriented polypropylene (BOPP) exhibited only a discharged energy density of 7.9 J cm^{-3} and 1.2 J cm^{-3}, respectively. This systematic study provides a new design paradigm to exploit PVDF-based dielectric polymers for capacitor applications.

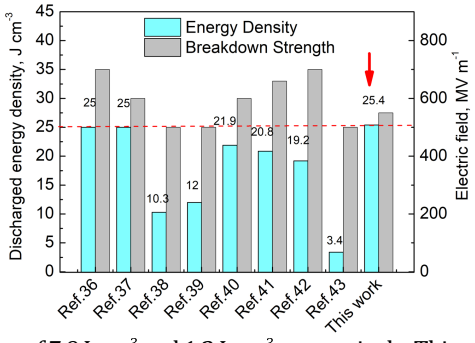

Keywords: biaxially oriented poly(vinylidene fluoride), high electric poling, high power-density capacitor, dielectric constant, ferroelectric crystalline phase.

1. Introduction

High-energy-density materials have been widely used in electronic and electrical devices such as electrostatic capacitors,[1-4] organic field-effect transistors[5,6] and nonvolatile memories.[7,8] From the past decades, biaxial-oriented polypropylene (BOPP) has been emerging as a novel polymer capacitor film due to excellent properties including lightweight, cost-effective, high breakdown strength, low dielectric permittivity, and very low dielectric loss.[9] Among polymer dielectric materials, poly(vinylidene fluoride)-based (PVDF-based) polymers have been noticed as an excellent candidate of dielectrics for capacitors because of high charge-discharge efficiency and high storage density.[10-12]

In order to improve the energy density of PVDF-based ferroelectric polymers, structural optimization can be an effective method. The crystalline structure can have a large impact on the electrical field-induced polarization response in the polymer dielectric materials. To be notable, PVDF homopolymer demonstrates the five polymorphs (α-, β-, γ-, δ-, and ε) phases with dissimilar unit cells of varying polarity. Typically, PVDF forms the most stable α-phase crystals composed by antiparallel dipoles in the non-polar domains (paraelectric crystalline domains), resulting in low polarization response in terms of low dielectric constant and low energy density.[13-15] Therefore, structural optimization can be considered a central topic in the field of electroactive applications based on the advanced dielectric properties.[16] So far, several chemical and physical ways have been explored, such as electron-irradiated,[17,18] co-polymerization,[19] graft polymerization,[20,21] cross-linking,[22] melt-stretching,[23,24] nanocomposites[25-27] and multilayer-architecture[28] to investigate varying crystalline structures and morphologies. Alit should be noticeable that electron-irradiated PVDF-trifluoroethylene (P(VDF-TrFE)) exhibits an elastic energy density greater than 10 J cm^{-3} with respect to P(VDF-TrFE), resulted from the effectively reduce dipolar coupling due to the chemical defects and irregular molecules induced by electron irradiation and then transformed ferroelectrics P(VDF-TrFE) into a ferroelectric relaxor. Further, the cross-linked networks between the PVDF-hexafluoropropyl-

Acknowledgments: This work was supported by National Natural Science Foundation of China (Grant No.51703044), the School Science Starting Foundation of Hangzhou Dianzi University (Grant No. KYS205617016), the Opening Project of Key Laboratory of Optoelectronic Chemical Materials and Devices, Ministry of Education, Jianghan University (No. JDGD-201804), and the Zhejiang Provincial Natural Science Foundation of China (Grant No. LY18E020005).

***Corresponding Author:** Yingxin Chen (yxchen@hdu.edu.cn)

ene (P(VDF-HFP)) and P(VDF-TrFE)-chlorofloroethylene (P(VDF-TrFE-CFE)) were reported, exhibits opposite results in the energy density and charged-discharged efficiency. It may be attributed to the cross-linking occurred in the crystalline regions of P(VDF-HFP), while the amorphous regions of P(VDF-TrFE-CFE) remained unchanged.[29] Recently, a novel architecture of trilayered for polymer nanocomposite with an optimized filler content demonstrated a discharged energy density of 20.5 J cm^{-3} at the maximum breakdown strength of 588 MV m^{-1}.[28]

Furthermore, the realization of ultra-high breakdown strength E_b, is another effective approach to enhance energy density. Typically, two-dimensional (2-D) hexagonal boron nitride (BNNS) with an electric field strength of 800 MV m^{-1} was used to enhance Weibull breakdown strength of PVDF-based nanocomposites at the expense of dielectric constant (K), leading to unprecedented energy storage capability.[30] Also, poly(methyl methacrylate) (PMMA) with a low K value was blended into poly(vinylidene fluoride) (PVDF), a significant improvement in the charge-discharge efficiency and breakdown strength was attained. However, this method usually results in decreased dielectric and energy storage densities.[31] Specifically, PMMA was used as the middle layer in the trilayered all-polymer film, resulted in improved charge-discharge efficiency (η) and the discharged energy density due to novel layered architecture.

In this paper, we carried out a simple and scalable method devoid of the high dielectric-constant or dielectric-strength nano-fillers to simultaneously improve dielectric constant and breakdown strength. An ultra-high energy density of BOPVDF film was achieved via poled at the various poling electric field. The dielectric and ferroelectric properties are studied comprehensively. An ultra-high energy density of 25.4 J cm^{-3} at the applied electric field of 550 MV m^{-1} was obtained in poled BOPVDF film on the counterpart of unpoled BOPVDF film and commercial BOPP film. Structural characteristics were explored using the X-ray diffractometer (XRD) tool. This work demonstrated that a suitable high electric poling nearly equal to the coercive electric field, can be increased the electric polarization by structural optimization and also enhanced breakdown strength. The presented systematic study can be worthwhile to reveal the structural factor to attain the high energy density for the capacitor applications.

2. Experimental

The biaxially oriented BOPVDF films as a sample were 9-μm-thick capacitor grade films produced by Technology Center at the Juhua Group Corporation.

High electric poling of the BOPVDF film was carried out as follows: Circular gold electrodes of a thickness of 60 nm and a diameter of 5 mm were deposited on both sides of BOPVDF film using metal vapor evaporator. Poling on the films was carried out by using a device connected to a DC power source by a pair of brass blocks. The PE film with a thickness of 44 μm was used as an insulating layer and tightly mounted on the lower brass block to reduce the possibility of flashover. The total thickness of films is about 53 μm. The films were immersed in the silicone oil for poling. During poling, a series of DC voltages of 0, 2000, 4000, and 6000 V corresponding to the electric field of 0, 38, 75, and 113 MV m^{-1} were applied on the BOPVDF film for one hour, which was named as P_0, P_1, P_2, and P_3, respectively.

2.1. Characterization

The dielectric permittivity of the prepared samples was examined at the testing frequency from 20 to 10^6 Hz via a high-precision LCR meter made by HP4284A; Agilent, Palo Alto, CA.

Ferroelectric properties were investigated by using Ferroelectric bipolar and unipolar P-E hysteresis loops obtained by using Radiant Technologies Precision Premier II, which was equipped with 10^4 V amplifiers at the testing frequency of 100 Hz. Electric breakdown strength measurements were carried out using a High Voltage Power Supply (DW-P503-1ACDFO).

2.2. Structure characterization

The crystalline structure was collected by X-ray diffractometer (XRD, Bruker-D8) at the 2θ range from 5-30°, and recorded by Fourier transform infrared spectroscopy (FTIR, Bruker Tensor) instrument from 4000 cm^{-1} to 400 cm^{-1}.

3. Results and discussion

PVDF-based polymers are promising semi-crystalline materials for electric energy storage and conversion.[44] These polymers exhibit high energy density, rapid polarization switching, large field-induced strain, and distinct electro-caloric effect.[45,46] In order to examine the energy charge-discharge behavior of PVDF film, a series of high DC voltages of 2000, 4000, and 6000 V corresponding to the electric field of 38, 75, and 113 MV·m^{-1} were applied on the BOPVDF films to tune the size of the ferroelectric domain and the C-F dipole direction. Thus high energy storage capacitance was achieved, as shown in Figure 1(a). The polycrystalline phases of BOPVDF films (P_0, P_1, P_2, and P_3) which poled

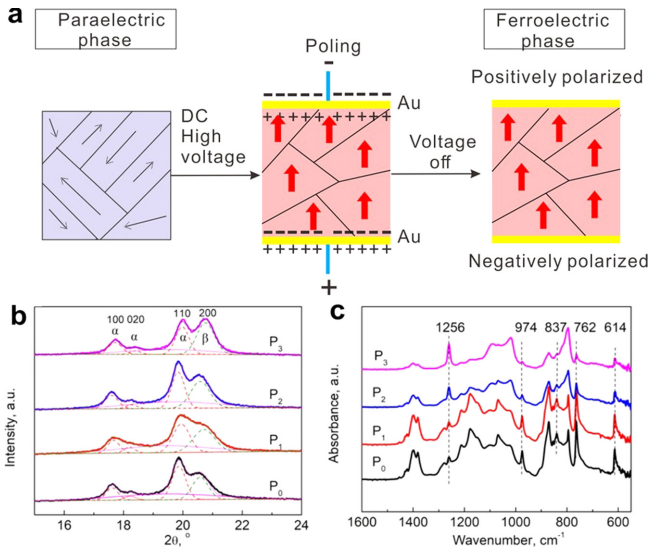

Figure 1. (a) The schematic images of the poling process of BOPVDF film under the DC high voltage, (b) XRD curves well fitted by Gaussian, and (c) FTIR spectra of the films P_0, P_1, P_2 and P_3.

at the varying electric field were further characterized by XRD, as shown in Figure 1(b). The unpoled BOPVDF shows three peaks at 17.7, 18.4, and 19.9°, which are ascribed to (100), (020), and (110) reflections of the paraelectric α-phase crystals, respectively. However, the peak at 20.8° is ascribed to (200) reflection of the ferroelectric β/γ-phase crystals. Notably, the crystalline structure of BOPVDF film is composed of paraelectric α-phase and ferroelectric β/γ-phase crystals. On gradually increasing poling electric field, the intensity of the diffraction peaking at 20.8° was increased, while it's suppressed at 19.9°, indicating that partial paraelectric α-phase crystals are transferred into the β/γ-phase crystals. Furthermore, the structural transformation between the paraelectric and ferroelectric crystals under the application of varying poling electric field is shown in Table 1. The sizes of ferroelectric and paraelectric crystals (L) are calculated by the Scherrer Eq. (1):

$$L = \frac{0.9\lambda}{B\cos\theta} \quad (1)$$

where λ, θ, and B is X-ray wavelength, angular position of the diffraction peaks and full width at half maximum, respectively.[32] The size of paraelectric crystals of 17.6 nm in the pristine BOPVDF is obtained, that larger than those of the poled film P_1 of 16.5 nm, P_2 of 16.0 nm and P_3 of 15.3 nm, respectively. On the other hand, the ferroelectric crystallites are formed with sizes from 9.2 nm to 11.5 nm, as shown in Table 1. It can be seen that the ratio of the integrated area between the two peaks ($R_{200/100}$) is also increased (Table 1). This phenomenon indicates that a large electric field can induce a change in the dipole orientations in the BOPVDF crystals, leading to the structural transformation of the α-phase crystals into the β-phase crystals.

In order to confirm the existence of the polymorphic crystalline phases, analysis of FTIR characterization was also included in this study, as shown in Figure 1(c). FTIR measurement was carried out using BOPVDF films under the varying poling electric field (P_0, P_1, P_2, and P_3). The bands at 1256 cm^{-1} ascribed to $T_{n>=4}G$ conformations in the β-phase crystals, enhance remarkably in intensity with the increasing of applied poling electric field. Although, the absorbance bands at 762 and 614 cm^{-1} for TGTG' conformation in the α-phase crystals decreases in turn, showing consistency with the XRD results.

Since most of the polarization response originates in the crystalline phase, varying the crystal structure and morphology of polymers through the applied high electric field poling can largely affect the polarization. The bipolar polarization *vs.* applied electric fields (*P-E*) hysteresis loops of the unpoled, P_0, and poled samples, including, P_1, P_2, and P_3, were measured, as shown in Figures 2(a)-(d). A sinusoidal electric field with a step of 20 MV m^{-1} and a testing frequency of 100 Hz was exerted across the BOPVDF film until the maximum electric coercive strength reached. For the BOPVDF film without poling, the oval-shaped *P-E* hysteresis loops which depict typical reversal behavior of the paraelectric crystals were observed. With the increasing poling electric field, a remnant polarization (P_r) (at E=0), a saturated polarization (P_s), and the coercive field (E_c) (at P=0) gradually enhance with the increasing electric field, as shown in Figure 2(a).

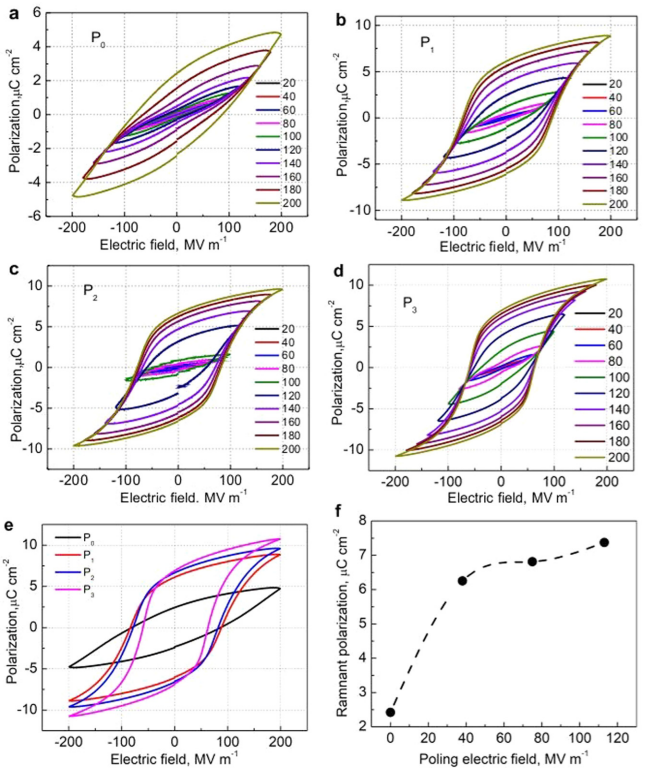

Figure 2. Ferroelectric *P-E* hysteresis loops of (a) original BOPVDF, (b) P_1, (c) P_2, and (d) P_3 under various poling electric fields. (e) Overlaid *P-E* hysteresis loops at the electric field of 200 MVm^{-1} for P_0, P_1, P_2, and P_3. (f) Remnant polarization of P_0, P_1, P_2, and P_3 as a function of the poling electric field.

As can be seen in Figures 2(b)-(d), after poling at the electric field of 38, 75, and 113 MVm^{-1}, the poled BOPVDF samples exhibit the large square-shaped *P-E* hysteresis loop with the larger P_r and P_s, and the lower E_c in the counterpart of the unpoled BOPVDF. It may be due to the applied high electric field poling can altered α-phase with TGTG' conformations to a polar β phase with TTTG conformations and γ-phase, supported by the abovementioned XRD results.[33] For instance, at the electric field of 200 MVm^{-1}, the value P_r, P_s, and E_c of the unpoled BOPVDF is 2.5 μC cm^{-2}, 4.7μC cm^{-2}, and 87 MVm^{-1}, as shown in Figure 2(e),

Table 1. The lattice constants (d) and sizes of ferroelectric and paraelectric crystals (L) for the reflections of (200) and (110) of BOPVDF films under the applied poling electric fields (P_0, P_1, P_2, and P_3) and the ratio of the integrated areas between two peaks ($R_{200/100}$)

	β-phase crystals		α-phase crystals		$R_{200/100}$
	D (Å) (200)	L (nm)	d (Å) (110)	L (nm)	
P_0	4.32	9.2	4.47	17.6	0.78
P_1	4.28	9.5	4.45	16.5	1.06
P_2	4.31	10.6	4.47	16.0	1.14
P_3	4.27	11.5	4.44	15.3	1.29

respectively. On the other hand, interestingly, the high electric field poling-assisted BOPVDF sample P_3 displays a maximum P_r of 7.2 μC cm^{-2} (Figure 2(f)), a maximum P_s of 10.7 μC cm^{-2} and a minimum E_c of 62.7 MVm^{-1}. The good ferroelectricity with largely saturated polarization was attained in the poled BOPVDF films, leading to advantageous to high-capacitance applications.

Dielectric and energy storage characteristics of the BOPVDF are explained using Figure 3. The charged-discharged energy density is calculated from unipolar *P-E* loops by the equation: $U=\int E\,dD$. *U*, charged energy density, is depend on the applied electric field, *E,* and electric displacement, *D*. For linear dielectrics, $U=½\,DE=½\,\varepsilon_r\varepsilon_0 E^2$, where ε_r and ε_0 are the permittivity of the dielectric and vacuum medium respectively. Therefore, charged-discharged energy density is closely related to the permittivity of dielectric medium, ε_r, and *E*. The size of the crystals as well as chain conformations was regulated by high electric field in order to achieve high dielectric constant and high discharged energy density. The dielectric permittivity and dielectric loss of the samples P_0-P_4 were measured as a function of frequency from 0.1 Hz to 10^6 Hz, as shown in Figure 3. The ε_r value decreases with the increasing frequency (Figure 2(a)) because of ferroelectric and nonlinear nature of the crystals. The unpoled film exhibited the lowest ε_r of ~8.5 at the frequency of 10^3 Hz as compared with other poled films. It may be due to the random CF_2 dipole orientation in the flat-on crystals, as shown in Figure 3(a). Therefore, the polarizability of dipole orientation in the crystals with the flat-on direction was low because it was difficult to be oriented along the applied electric field.[4] However, the dipole moments of CF_2 in the poled BOPVDF crystals were distributed along the plane parallel to the electric field and the sizes of the ferroelectric crystals with all-trans conformation grew larger, as can be seen in Figure 3(a). Thus, it is demonstrated that the polarizability of the dipole orientation in the ferroelectric crystals strongly depends on the poling electric field. The poled film of the sample P_3 showed the highest ε_r of ~14.5 at the frequency of 1000 Hz.

Additionally, the BOPVDF film poled in the various electric field was measured at the testing frequency ranges from 100 Hz to 1 MHz, and the curves are shown in Figure 3(b). It is generally known that dielectric loss is related to the origin of the varying dipole moments at the applied different frequencies.[31,34] At the testing frequency below 10^3 Hz, the low dielectric loss was observed in the poled films due to high interfacial polarization. In the poled films, the chains of PVDF were aligned perpendicular to the direction of an applied electric field, causing large ferroelectric phase formation by the application of the high poling electric field, and resulted in the lowest dielectric loss at the low frequency. Although, a little variation in the frequency range up to 10^5 Hz increases to a sharp peak around 10^6 Hz can be obtained.[35] Also, with the increasing poling electric field, limited interface areas were formed in the poled films than that of the unpoled film P_0. It can be another reason for the low dielectric loss.

To examine the influence of the poling electric field on the breaking down of the films, E_b of BOPVDF films were obtained, and the obtained data were analyzed within the framework of Weibull statistics, as explained by the Eq. (2):

$$P = 1 - \exp(-(\frac{E}{\alpha})^{\beta}) \quad (2)$$

where, *P*, E_b, α, and β is ascribed to the cumulative probability of the electric failure, the measured breakdown field, Weibull breakdown strength, and the scatter of data, respectively. The characteristic E_b of the BOPVDF films poled at the varying electric field from 0 to 113 MVm^{-1} is analyzed, as shown in Figures 4(a) and 4(b). Initially, E_b is firstly enhanced upon the increasing poling electric field from 0 to 38 MVm^{-1}, and then reduces beyond the electric field of 38 MVm^{-1}. The applied electric field lower than the coercive field (E_c) is effective in adjusting the molecular chains to form the ferroelectric β-form crystals. Although, the high electric polarization was obtained in the BOPVDF film when the electric field is far larger than E_c. It resulted in enhanced the probability of breakdown strength and the value of E_b decreases from 491 to 375 MVm^{-1}. It may be attributed to the excessive injection of charge.

The unipolar charge-discharge cycles were applied in a step of the electric field of 50 MVm^{-1} until the maximum breakdown electric field. The obtained *P-E* curves are shown in Figure 5. With the gradual enhancement in electric field strength, the polarization of BOPVDF reaches up to the maximum value, demonstrates the storage of electric energy into the BOPVDF. And the continuous decrease of field strength leads to the release of electrical energy from the BOPVDF. The unpoled BOPVDF film exhibits the maximum electric field of 310 MV and the maximum polarization value of 5.5 μC cm^{-2} before the breakdown. Surprisingly, the poled BOPVDF film P_2 shows a relatively high electric field of 550 MV m^{-1} and the maximum value of 7.3 μC cm^{-2}, indicating

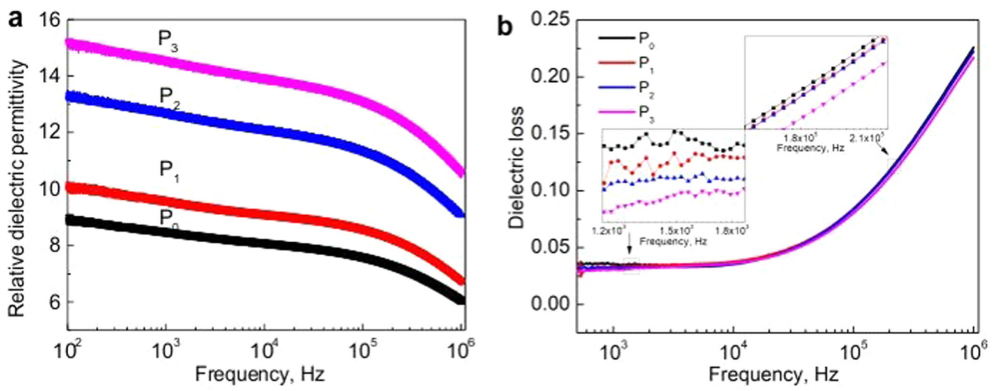

Figure 3. (a) Relative dielectric permittivity, and (b) dielectric loss of BOPVDF (P_0), P_1, P_2, and P_3 measured from 0.1 kHz to 1 MHz, and the enlarged plots for the specific frequency ranges in the insets.

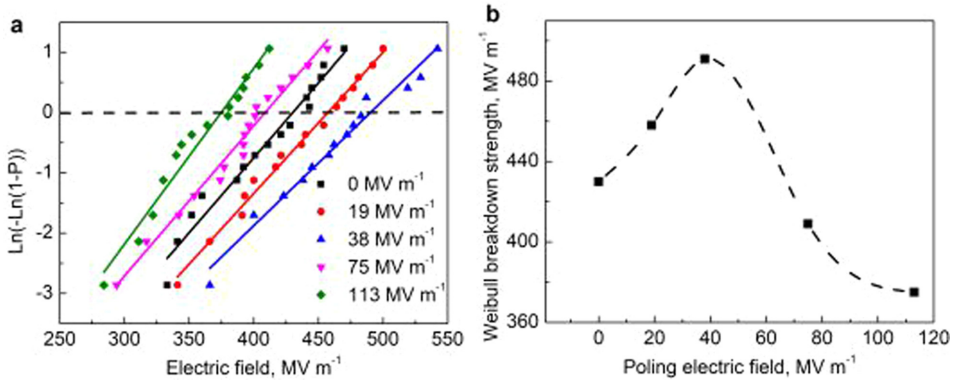

Figure 4. (a) Weibull plots for the film of BOPVDF poled with the electric field of 0, 19, 38, 75, and 113 MV m^{-1}. (b) Weibull breakdown strength of BOPVDF as a function of poling electric field.

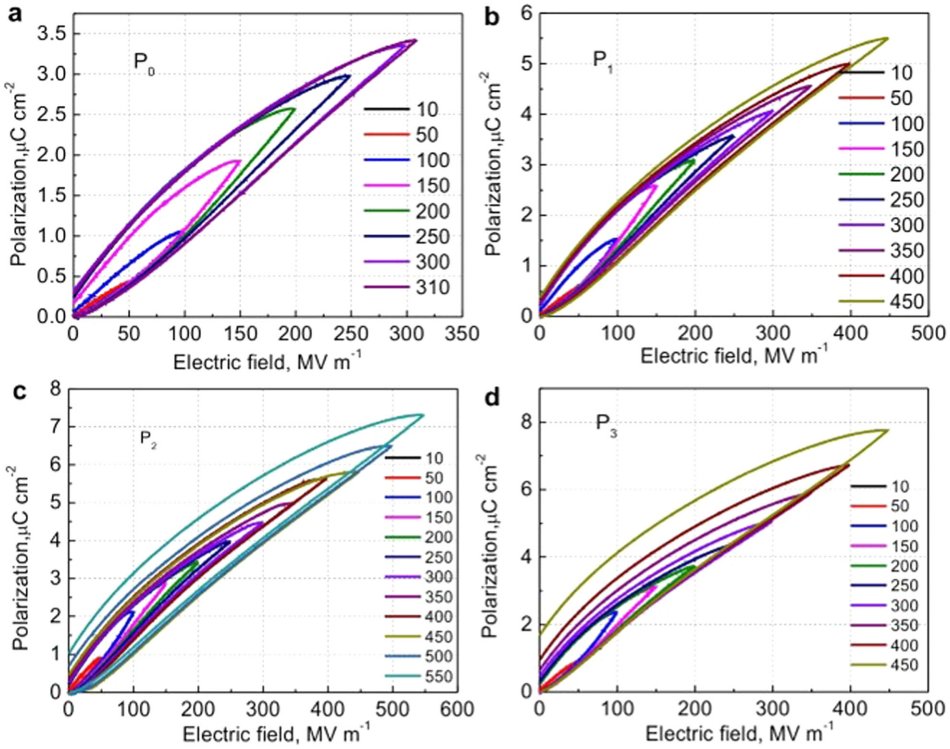

Figure 5. *P-E* hysteresis curves of (a) P_0, (b) P_1, (c) P_2, and (d) P_3 (before breakdown).

high energy storage capacitance.

Figure 6(a) shows the unipolar *P-E* hysteresis loops of P_0, P_1, P_2, and P_3 at the same electric field. Initially, high electric poling has an obvious effect on the *P-E* loops, causing increased polarization slope and hysteresis. Under the application of the electric field, the polarization increases with the increasing electric field. Importantly, when the electric field was reduced to 0 MV·m^{-1}, the poled BOPVDF film (P_3) showed the highest remnant polarization of 0.49 μC/cm^2. At the applied electric field of 300 MVm^{-1}, the unpoled BOPVDF (P_0) exhibits a relatively low level of the polarization about 3.4 μC/cm^2, however, the value of P_1, P_2, and P_3 reaches to 4.0, 4.5, and 5.1 μC/cm^2, respectively. The enhancement of electric displacement and remnant polarization value may be closely relevant to that high electric field of poling BOPVDF that helps to form the larger size of the ferroelectric crystals with all-trans conformation.

The charged and discharged energy density ($U_{charged}$ and $U_{discharged}$) can be integrated from the unipolar *P-E* loops, as shown in Figure 6(b) and 6(c). Thereafter, the charged-discharged efficiency was defined as $U_{discharged}/U_{charged}$. The calculated results were shown in Figure 6(d). The charged and discharged energy density as a function of the electric field were recorded as gradual and monotonic. First, the unpoled film P_0 showed the lowest charged and discharged energy density of 9.8 Jcm^{-3} and 7.9 J cm^{-3} at the electric field of 310 MVm^{-1}, respectively. It may be due to the normal direction of ferroelectric domains in the unpoled BOPVDF film that is perpendicular to the poling direction, inhibiting high electric polarization. Further, at the electric field of 450 MV m^{-1}, the poled BOPVDF film P_3 exhibited the higher charged and discharged energy densities of 26 J cm^{-3} and 18.3 J cm^{-3} with respect to the poled film P_1 (21.2 J cm^{-3} and 17.6 J cm^{-3}), respectively. Interestingly, the highest charged and discharged energy density of 33.3 J cm^{-3} and 25.4 J cm^{-3} was attained in the poled film P_2, which is 20 times more than that of the commercial

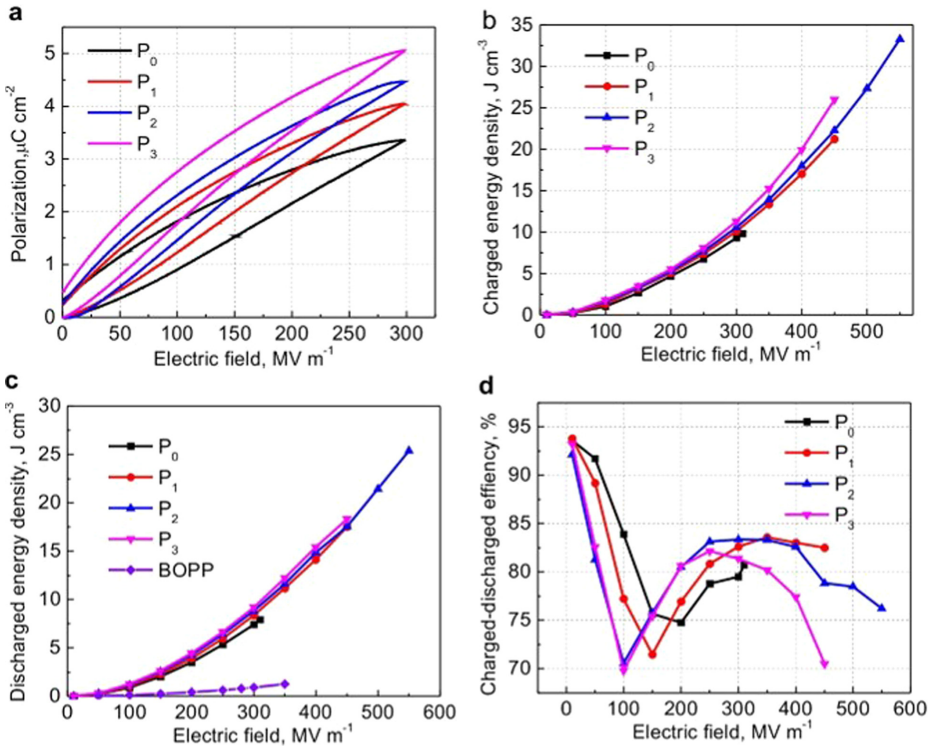

Figure 6. (a) The comparison of *P-E* hysteresis loops at the same electric field, (b) charged energy density, (c) discharged energy density, and (d) charge-discharge efficiency of P_0, P_1, P_2, P_3, and BOPP as a function of the field strength.

BOPP, as shown in Figure 6(c). It can be explained by the orientation of the large dipoles. The large dipoles in the crystals begin to orient under high electric field, and thus form ferroelectric crystals with more parallel to the poling direction. It is the fundamental reason for the tremendous increase in energy density.

From the perspective of the capacitor, the charge-discharge efficiency is also important to affect the reliability of the capacitor because of the thermal energy.[44] As shown in Figure 6(d), a steep decline in the capacitor efficiency was observed in the all samples when the electric field increases up to 100 MV m^{-1}, and then the increasing trend in the discharged efficiency from 100 MV m^{-1} to 300 MV m^{-1}. Finally, the dramatic decrease of energy efficiency is due to conduction loss was observed at the applied electric field beyond 300 MV m^{-1}. At the low electric field, the poled BOPVDF films (P_1, P_2, and P_3) exhibited lower discharged efficiency with respect to the unpoled film (P_0) because of the dominant effect of the ferroelectric loss in the poled samples. However, the poled BOPVDF films showed higher discharged efficiency than that of the unpoled BOPVDF. It may be attributed to the high conduction loss in the unpoled sample at the high electric field. Therefore, the poled films with high charged-discharged efficiency at the high electric field are beneficial for improving the reliability of high-energy-density capacitors.

Discharged energy density and the breakdown strength of the poled BOPVDF and other PVDF-based dielectric materials[36-43] are shown in Figure 7. Previous studies have shown that a high energy density of 25 J cm^{-3} was attained in the P(VDF-CTFE) and P(VDF-HFP) copolymers, but the maximum breakdown strength of P(VDF-HFP) (700 MV m^{-1}) was higher than that of P(VDF-CTFE) (600 MV m^{-1}) because of low electric polarization of P(VDF-CTFE).[37] Furthermore, the blending of low-electric-polarization of PEMA and ArPTU can obviously reduce the polar-

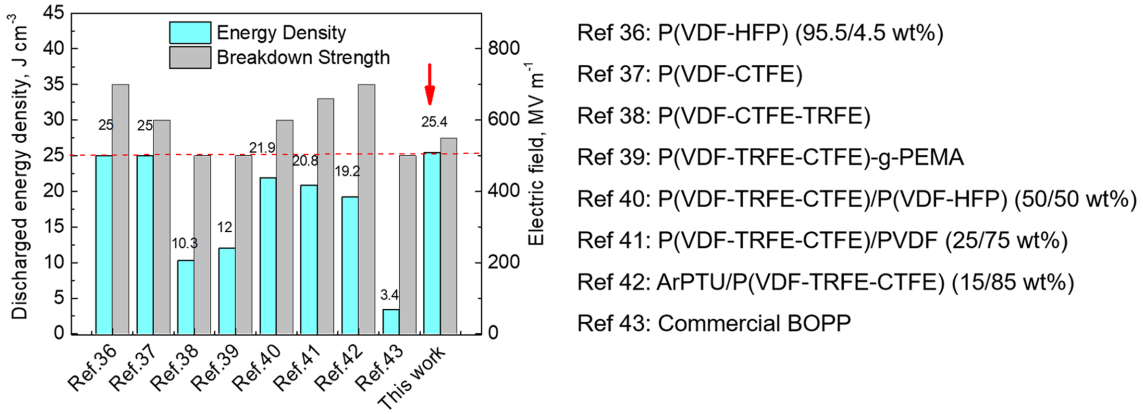

Figure 7. The comparison of discharged energy density and breakdown strength between the poled BOPVDF and other polymer-based dielectric materials reported in the corresponding references.

ization as well as low energy density.[39] For instance, ultra-high electric strength of 700 MV m^{-1} was achieved, although, discharged energy density of ArPTU/P(VDF-TrFE-CTFE) was only 19.2 J cm^{-3}. In the relaxor ferroelectrics P(VDF-TrFE-CTFE), a very high dielectric constant and low electric polarization is not a desirable feature for a dielectric material to achieve a very-high energy density. In our study, a suitable poling electric field was applied to the BOPVDF films, resulting in improving the electric polarization in high breakdown strength *i.e.* ultrahigh energy density was achieved. Remarkably, the poled BOPVDF film at the electric field of 113 MV m^{-1} exhibited an unprecedented discharged energy density of 25.4 J cm^{-3} at an ultra-high electric field of 550 MV m^{-1} that is the highest value ever achieved in flexible polymer-based capacitor films.

4. Conclusions

In this study, high-electric field poling assisted different C-F dipole-oriented PVDF crystals were studied to explore the corresponding dielectric constants and energy storage characteristics. The high electric poling-assisted BOPVDF films composed by the larger ferroelectric crystals that were perpendicular to the electric field exhibited the higher dielectric constants and electric energy densities than that of the unpoled BOPVDF film. The recorded enhancement in the dielectric constant and electric polarization in the poled BOPVDF films may be closely related to the structural transformation from partial paraelectric α-phase crystals into the ferroelectric β/γ-phase crystals at the applied high electric field. This behavior of unpoled and poled BOPVDF films was confirmed by analyzing the XRD and FTIR plots. In addition, a suitable poling electric field to the BOPVDF films can be effective to enhance the breakdown strength. An ultrahigh discharged energy density of 25.4 J cm^{-3} at a high breakdown strength of 550 MV m^{-1} in the poled BOPVDF film was achieved. Our systematic studies provided in-depth understanding for the practical application of PVDF-based polymers for capacitor applications.

References

(1) B. J. Chu, X. Zhou, K. L. Ren, B. Neese, M. R. Lin, Q. Wang, F. Bauer, and Q. M. Zhang, *Science*, **313**, 334 (2006).
(2) Y. Xie, Y. Yu, Y. Feng, W. Jiang, and Z. Zhang, *ACS Appl. Mater. Interfaces*, **9**, 2995 (2017).
(3) X. Zhang, Y. Shen, B. Xu, Q. Zhang, L. Gu, J. Jiang, J. Ma, Y. Lin, and C. W. Nan, *Adv. Mater.*, **28**, 2055 (2016).
(4) F. Guan, J. Pan, J. Wang, Q. Wang, and L. Zhu, *Macromolecules*, **43**, 384 (2010).
(5) G. Yunlong, Y. Gui, and L. Yunqi, *Adv. Mater.*, **22**, 4427 (2010).
(6) D. Chong-an, Z. Fengjiao, and Z. Daoben, *Adv. Mater.*, **25**, 313 (2013).
(7) X.-Z. Chen, Q. Li, X. Chen, X. Guo, H.-X. Ge, Y. Liu, and Q.-D. Shen, *Adv. Funct. Mater.*, **23**, 3124 (2013).
(8) Y. Chen, X. Chen, H. Lu, L. Zhang, Y. Yang, and Q.-D. Shen, *Polymer*, **143**, 281 (2018).
(9) H. Tang and H. A. Sodano, *Nano Lett.*, **13**, 1373 (2013).
(10) M. Rabuffi and G. Picci, *IEEE T. Plasma. Sci.*, **30**, 1939 (2002).
(11) L. A. Fredin, Z. Li, M. A. Ratner, M. T. Lanagan, and T. J. Marks, *Adv. Mater.*, **24**, 5946 (2012).
(12) W. Xu, G. Yang, L. Jin, J. Liu, Y. Zhang, Z. Zhang, and Z. Jiang, *ACS Appl. Mater. Interfaces*, **10**, 11233 (2018).
(13) A. J. Lovinger, *Science*, **220**, 1115 (1983).
(14) A. J. Lovinger, D. Davis, R. Cais, and J. Kometani, *Polymer*, **28**, 617 (1987).
(15) F. B. Calleja, A. G. Arche, T. Ezquerra, C. Santa Cruz, F. Batallan, B. Frick, and E. L. Cabarcos, in *Structure in Polymers with Special Properties*, Springer, 1993, pp 1-48.
(16) G. R. Li, N. Kagami, and H. Ohigashi, *J. Appl. Phys.*, **72**, 1056 (1992).
(17) Q. M. Zhang, *Science*, **280**, 2101 (1998).
(18) Q. M. Zhang, Z.-Y. Cheng, and V. Bharti, *Appl. Phys. A*, **70**, 307 (2000).
(19) Z. Zhang and T. C. M. Chung, *Macromolecules*, **40**, 783 (2007).
(20) X. Chenyang, L. Jingye, Y. Chunming, and L. Yongjin, *Macromol. Rapid Commun.*, **37**, 1559 (2016).
(21) F. Guan, L. Yang, J. Wang, B. Guan, K. Han, Q. Wang, and L. Zhu, *Adv. Funct. Mater.*, **21**, 3176 (2011).
(22) C. Yingxin, T. Xin, S. Jie, W. Xiaoliang, H. Wenbing, and S. Qun-Dong, *J. Polym. Sci. Part B: Polym. Phys.*, **54**, 1160 (2016).
(23) B. Mohammadi, A. A. Yousefi, and S. M. Bellah, *Polym. Test.*, **26**, 42 (2007).
(24) L. Yang, J. Ho, E. Allahyarov, R. Mu, and L. Zhu, *ACS Appl. Mater. Interfaces*, **7**, 19894 (2015).
(25) H. Xingyi and J. Pingkai, *Adv. Mater.*, **27**, 546 (2015).
(26) Y. Li, X. Huang, Z. Hu, P. Jiang, S. Li, and T. Tanaka, *ACS Appl. Mater. Interfaces*, **3**, 4396 (2011).
(27) C. Xing, L. Zhao, J. You, W. Dong, X. Cao, and Y. Li, *J. Phys. Chem. B*, **116**, 8312 (2012).
(28) L. Feihua, L. Qi, C. Jin, L. Zeyu, Y. Guang, L. Yang, D. Lijie, X. Chuanxi, W. Hong, and W. Qing, *Adv. Funct. Mater.*, **27**, 1606292 (2017).
(29) Y. X. Chen, Z. X. Cheng, and Q. D. Shen, *IEEE Trans. Dielectr. Electr. Insul.*, **24**, 682 (2017).
(30) Q. Li, K. Han, M. R. Gadinski, G. Z. Zhang, and Q. Wang, *Adv. Mater.*, **26**, 6244 (2014).
(31) Q. Meng, W. Li, Y. Zheng, and Z. Zhang, *J. Appl. Polym. Sci.*, **116**, 2674 (2010).
(32) R. J. Klein, J. Runt, and Q.-M. Zhang, *Macromolecules*, **36**, 7220 (2003).
(33) Z. Zhang and T. C. M. Chung, *Macromolecules*, **40**, 9391 (2007).
(34) L. L. Sun, B. Li, Y. Zhao, G. Mitchell, and W. H. Zhong, *Nanotechnology*, **21**, 305702 (2010).
(35) B. Hahn, J. Wendorff, and D. Y. Yoon, *Macromolecules*, **18**, 718 (1985).
(36) X. Zhou, X. Zhao, Z. Suo, C. Zou, J. Runt, S. Liu, S. Zhang, and Q. M. Zhang, *Appl. Phys. Lett.*, **94**, 162901 (2009).
(37) X. Zhou, B. Chu, B. Neese, M. Lin, Q. M. Zhang, *IEEE Trans. Dielectr. Electr. Insul.*, **5**, 1133 (2007).
(38) Z. Zhang, Q. Meng, and T. C. Mike Chung, *Polymer*, **50**, 707 (2009).
(39) J. Li, X. Hu, G. Gao, S. Ding, H. Li, L. Yang, and Z. Zhang, *J. Mater. Chem. C*, **1**, 1111 (2013).
(40) X. Ren, N. Meng, H. Yan, E. Bilotti, and M. J. Reece, *Polymer*, **168**, 246 (2019).
(41) L. Wang, H. Luo, X. Zhou, X. Yuan, K. Zhou, and D. Zhang, *Compos. Part A,* **117**, 369 (2019).
(42) H. Zhu, Z. Liu, and F. Wang, *J. Mater. Sci.*, **52**, 5048 (2017).
(43) Y. F. Wang, L. X. Wang, Q. B. Yuan, J. Chen, Y. J. Niu, X. W. Xu, Y. T. Cheng, B. Yao, Q.Wang, and H. Wang, *Nano Energy*, **44**, 364 (2018).
(44) Y. X. Chen, Y. F. Yue, J. Liu, J. Shu, A. P. Liu, B. J. Chu, M. H. Xu, W. Z. Xu, T. Chen, J. Zhang, and Q. D. Shen, *Phys. Chem. Chem. Phys.*, **21**, 20661 (2019).
(45) Y. X. Chen, L. Zhang, J. H. Liu, X. L. Lin, W. Z. Xu, Y. F. Yue, and Q. D. Shen, *Carbon*, **144**, 15 (2019).
(46) G. Zhang, Q. Li, H. Gu, S. Jiang, K. Han, M. R. Gadinski, M. A. Haque, Q. Zhang, and Q. Wang, *Adv. Mater.*, **27**, 1450 (2015).

